ARTICLE

doi:10.1038/nature11331

Passenger deletions generate therapeutic vulnerabilities in cancer

Florian L. Muller[1,2,3]*, Simona Colla[1,2,3]*, Elisa Aquilanti[2]*, Veronica E. Manzo[2], Giannicola Genovese[1,2], Jaclyn Lee[2], Daniel Eisenson[2], Rujuta Narurkar[2], Pingna Deng[1,2], Luigi Nezi[1,2], Michelle A. Lee[2,4], Baoli Hu[1,2,5], Jian Hu[1,2,3], Ergun Sahin[2,3], Derrick Ong[1,2,3], Eliot Fletcher-Sananikone[1,2], Dennis Ho[2,3], Lawrence Kwong[1,2], Cameron Brennan[6], Y. Alan Wang[1,2,5], Lynda Chin[1,2,5] & Ronald A. DePinho[2,3,5,7]

Inactivation of tumour-suppressor genes by homozygous deletion is a prototypic event in the cancer genome, yet such deletions often encompass neighbouring genes. We propose that homozygous deletions in such passenger genes can expose cancer-specific therapeutic vulnerabilities when the collaterally deleted gene is a member of a functionally redundant family of genes carrying out an essential function. The glycolytic gene enolase 1 (*ENO1*) in the 1p36 locus is deleted in glioblastoma (GBM), which is tolerated by the expression of *ENO2*. Here we show that short-hairpin-RNA-mediated silencing of *ENO2* selectively inhibits growth, survival and the tumorigenic potential of *ENO1*-deleted GBM cells, and that the enolase inhibitor phosphonoacetohydroxamate is selectively toxic to *ENO1*-deleted GBM cells relative to *ENO1*-intact GBM cells or normal astrocytes. The principle of collateral vulnerability should be applicable to other passenger-deleted genes encoding functionally redundant essential activities and provide an effective treatment strategy for cancers containing such genomic events.

Large-scale analysis of the cancer genome has provided an unprecedentedly detailed picture of the genetic anatomy of cancer[1], which has been, and continues to serve as, a blueprint for the development of molecular-targeted therapies. Targeted therapies directed against amplified or mutant-activated key driver oncoproteins have provided encouraging clinical progress[2], whereas exploiting loss-of-function mutations or gene deletions has received considerably less attention and has not been as successful thus far. Previous therapeutic work in the area of loss-of-function mutations and deletions has focused specifically on tumour-suppressor genes by strategies that include synthetic lethal approaches. One notable example of a synthetic lethal interaction is the response of BRCA1-mutant cancers to poly(ADP-ribose) polymerase inhibitors, although this interaction seems to be dependent on genetic context[3,4], and can be bypassed in late-stage tumours[3–5]. Most other synthetic lethal interactors of inactivated tumour suppressors seem to be less robust in eliciting cancer cell death[5], perhaps because such genes typically do not perform fundamental housekeeping functions.

Cancer genomes are characterized by numerous copy number amplifications and deletions, which target driver oncogenes and tumour-suppressor genes, respectively. Often, these genomic alterations are large regional events, affecting many other genes in addition to the intended target(s). The fact that such broad genomic alterations are not negatively selected against in cancer cells indicates that, on their own, the copy number alterations of these neighbouring passengers must not carry severely detrimental biological consequences. That said, it is conceivable that these passenger genomic events can create unintended (collateral) vulnerabilities unique to those cells; such as when a passenger being co-deleted is a member of a redundant multigene family serving an essential housekeeping function. A large body of genetic interaction studies in invertebrates as well as mice indicates that many essential cellular housekeeping functions are carried out by several homologous genes that encode overlapping functions; this redundancy enables cell viability after loss of one homologue but causes lethality after the loss of several homologues[6–10] (Supplementary Fig. 1). In this conceptual framework, we proposed that the homozygous deletion of redundant essential housekeeping genes could create cancer-specific vulnerabilities (Supplementary Fig. 1a), in which pharmacological inactivation of the second, non-deleted homologue would result in the complete loss of activity in tumour cells carrying the deletion, without compromising the health of normal cells, in which both genes are intact and expressed (Supplementary Fig. 1b).

ENO1 is a redundant housekeeping gene deleted in GBM

By examining The Cancer Genome Atlas (TCGA) GBM data set for homozygous deletions targeting genes involved in essential cell activities[1], we identified various such candidates, including the *ENO1* gene, which resides at the 1p36 tumour-suppressor locus (see Table 1 for a summary and Supplementary Table 1 for more detailed methodological support). Enolase, which is encoded by three homologous genes, is an essential enzyme that catalyses the second to last step of glycolysis, converting 2-phosphoglyceric acid into phosphoenolpyruvate[11]. In mammals, enolase activity is encoded by three genes: *ENO1*, which is ubiquitously expressed[12,13]; *ENO2*, which is expressed exclusively in neural tissues[12,14]; and *ENO3*, which is expressed in muscle tissues[15] (Supplementary Table 2). *ENO1* is the major enolase isoform in GBM, accounting for 75–90% of cellular enolase activity[12]. Given the crucial importance of glycolysis for energy generation and anabolic processes in normal and especially tumour cells[16], GBM tumours homozygous null for *ENO1* would be predicted to be highly sensitive to the inhibition of enolase 2, whereas

[1]Department of Genomic Medicine, University of Texas MD Anderson Cancer Center, Houston, Texas 77030, USA. [2]Department of Medical Oncology, Dana-Farber Cancer Institute, Boston, Massachusetts 02115, USA. [3]Department of Genetics and Medicine, Harvard Medical School, Boston, Massachusetts 02115, USA. [4]Department of Pediatric Oncology, Dana-Farber Cancer Institute, Boston, Massachusetts 02115, USA. [5]Belfer Institute for Applied Cancer Science, Dana-Farber Cancer Institute, Boston, Massachusetts 02115, USA. [6]Department of Neurosurgery, Memorial Sloan Kettering Cancer Center, New York, New York 10065, USA. [7]Department of Cancer Biology, University of Texas MD Anderson Cancer Center, Houston, Texas 77030, USA.
*These authors contributed equally to this work.

Table 1 | Homozygously deleted essential-redundant genes in GBM

Homozygously deleted gene	Chromosomal locus	Proximal tumour-suppressor gene	Target homologue	Pathway
ENO1	1p36.2	Various	*ENO2*	Glycolysis and gluconeogenesis
H6PD	1p36.2	Various	*G6PD*	Pentose phosphate shunt
KIF1B	1p36.2	Various	*KIF1A/C*	Chromosomal seggregation
NMNAT1	1p36.2	Various	*NMNAT2/3*	NAD^+ biosynthesis
UBE4B	1p36.2	Various	*UBE4A*	Polyubiquitin-dependent degradation
ACO1	9p21.*1*	*INK/ARF*	*ACO2/3*	Regulation of iron metabolism/citric acid cycle
KLHL9	9p22	*INK/ARF*	*KLHL13*	Chromosomal segregation
PANK1	10q23.31	*PTEN*	*PANK3*	Acetyl-CoA biosynthesis
KIF20B	10q23.31	*PTEN*	*KIF20A*	Chromosomal segregation/cytokinesis

An evidence-based filtered list of genes homozygously deleted in GBM that are likely to execute an essential housekeeping function and have redundant (and potentially druggable) homologues. A more detailed methods description is provided in Supplementary Table 1.

normal neural tissues should not be affected because of the functional redundancy of enolase 1 (Fig. 1a, b). Correspondingly, *Eno2* knockout mice are viable and fertile, suggesting that pharmacological inhibition of enolase 2 is likely to be well tolerated at the organism level (Supplementary Table 2). Moreover, *Saccharomyces cerevisiae*, which possesses several enolase homologues, shows weak phenotypes with single mutants and incurs cell lethality only when all homologues are deleted[8–10]; whereas *Caenorhabditis elegans* and *Drosophila* possess only one gene encoding enolase activity, and its deletion is lethal[17,18].

The 1p36 locus, which contains several candidate tumour-suppressor genes, including *CHD5* and *CAMTA1* (refs 19, 20), sustains frequent deletion in GBM (Fig. 2a). The 1p36 locus is homozygously deleted in 1–5% of GBMs[1,21,22] (as well as oligodendrogliomas[23] and large-cell neuroendocrine lung tumours[24]), and *ENO1* is often included in the deletion. By examining the TCGA copy number aberrations (single nucleotide polymorphism (SNP) and array comparative genomic hybridization (aCGH) data)[1] and expression profiles, we identified 5 out of 359 GBM samples with homozygous deletion of *ENO1* and associated near-complete absence of its expression (Fig. 2b and Supplementary Fig. 2). We identified two GBM cell lines, D423-MG[22] and Gli56 (ref. 25), with homozygous deletions at the 1p36 locus spanning *ENO1*. A third GBM cell line, D502-MG[22], also incurs homozygous deletion of many genes in this locus but not *ENO1*, thus serving as an excellent control (Fig. 2c). Western blot analysis confirmed the loss of ENO1 and the retention of ENO2 protein in D423-MG and Gli56 cells, whereas both proteins were present in D502-MG and in all other glioma and normal glial cell lines tested (Fig. 2d).

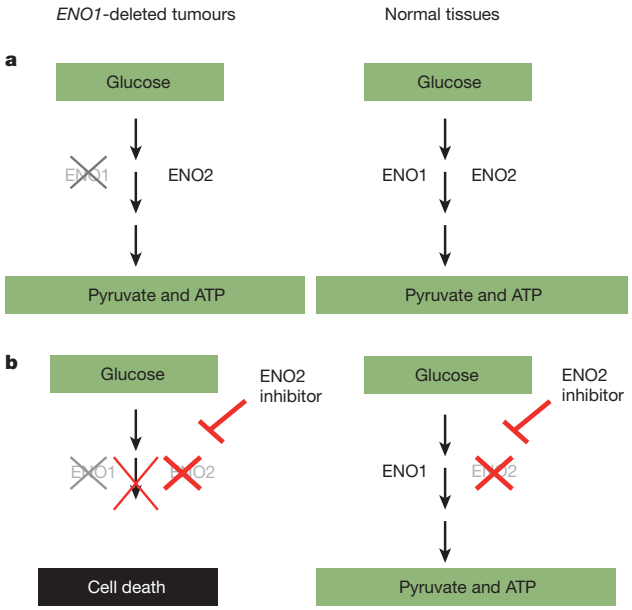

Figure 1 | Homozygous deletions in *ENO1* sensitize tumours to molecular targeting of ENO2. a, *ENO1* is homozygously deleted in glioblastomas as part of the 1p36 locus. Loss of ENO1 is tolerable to the tumour because ENO2 is still expressed. **b**, A specific ENO2 inhibitor should completely eliminate enolase activity in *ENO1*-null tumour cells (hence blocking glycolysis and ATP synthesis), but leave genomically intact normal tissues unaffected because enolase activity is still present as ENO1 is still expressed.

ENO2 knockdown inhibits growth of *ENO1*-deleted cells

We used the D502-MG (*ENO1* expressing) and D423-MG (*ENO1*-null) cell lines to assess the impact of short hairpin RNA (shRNA)-mediated knockdown of *ENO2* in an *ENO1* wild-type or null context. Two independent *ENO2* shRNAs (pLKO.1 vector) resulted in robust protein reduction and led to a profound inhibition of cell growth only in the context of *ENO1* genomic deletion (Supplementary Fig. 3). We obtained the same result using a further, independent *ENO2* shRNA (pGIPZ vector) (Supplementary Fig. 4a, b). Furthermore, shRNA ablation of *ENO2* in *ENO1*-null cells also resulted in decreased soft agar colony formation and blocked the *in vivo* tumorigenic potential of intracranially injected cells (Fig. 2e and Supplementary Fig. 4c). Finally, the selective toxicity of *ENO2* ablation to *ENO1*-null cells was demonstrated in an isogenic context using the doxycycline-inducible TRIPZ vector. When we used this doxycycline-inducible system in *ENO1* wild-type cell lines (U87, A1207 and LN319), two independent shRNAs reduced ENO2 protein levels by >70% (Fig. 3a) with no impact on ENO1 levels (data not shown). This *ENO2* ablation resulted in a profound inhibition of cell proliferation only in the *ENO1*-null D423-MG cell line (Fig. 3b). Furthermore, enforced expression of hairpin-resistant *ENO2* open reading frame fully reversed the deleterious effects of the *ENO2* shRNA (Supplementary Fig. 5), showing that the inhibitory effect of the hairpin was indeed specific to diminished ENO2 expression and was not an off-target effect. Finally, when ENO1 was ectopically re-expressed in D423-MG (*ENO1*-null) cell lines at levels similar to those observed in *ENO1* wild-type GBM lines, the deleterious effect of shRNA ablation of ENO2 was completely abrogated (Supplementary Fig. 6).

Enolase inhibition is toxic to *ENO1*-null cells

Next, we assessed the effect of pharmacological inhibition of enolase activity in *ENO1* wild-type and null cells. Previous studies have focused on the pharmacological inhibition of enolase, in particular for antiparasitic purposes[26,27], and many compounds have been characterized, most of which act as reaction-intermediate analogues (Supplementary Table 3). The most potent enolase inhibitor is phosphonoacetohydroxamate (PHAH)[27], which is thought to act as a transition-state analogue with an inhibitory constant of 15 pM on yeast enolase. Although PHAH has not been tested on human enolases, previous work demonstrated inhibitory effects on enolases from distantly related organisms[27,28], suggesting its potential use over a large phylogenetic distance. We find that PHAH was indeed capable of potent inhibition of enolase *in vitro* in native lysates of human GBM cell lines, with a half-maximum inhibitory concentration (IC_{50}) of around 20 nM (Fig. 4b and data not shown). We used PHAH in concentrations ranging from 0.625 μM to 50 μM and

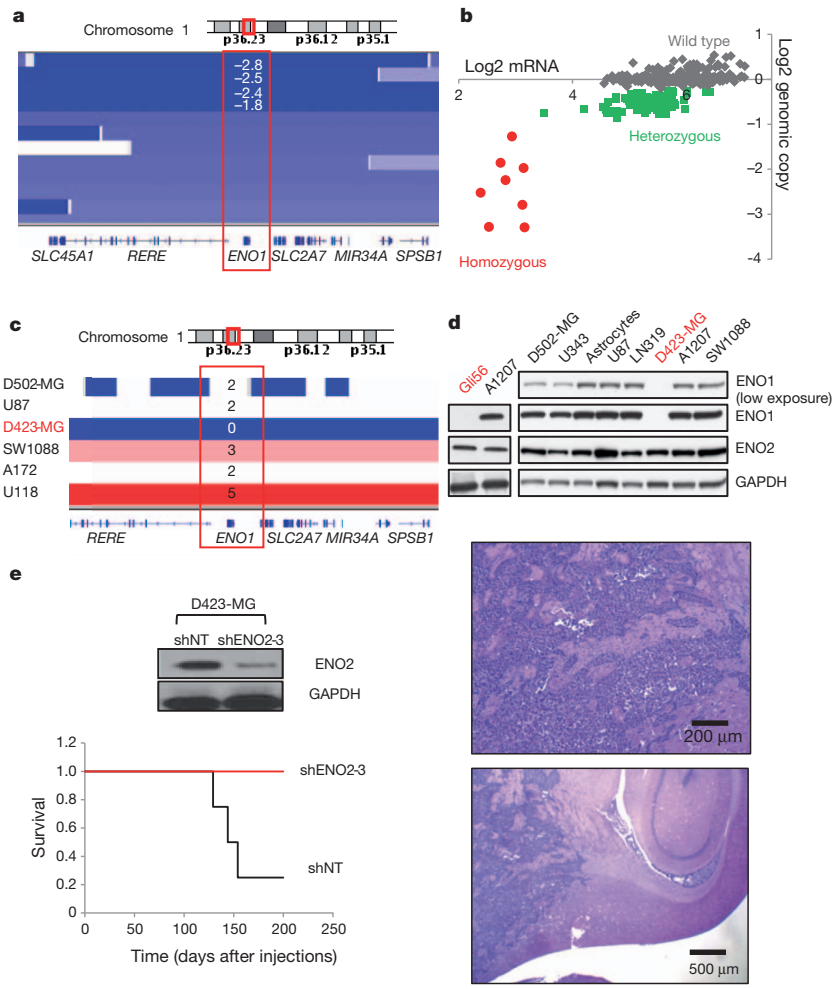

Figure 2 | Homozygous deletion of the 1p36 locus in GBM results in loss of *ENO1* expression in primary tumours and cell lines. **a**, TCGA aCGH data show four primary GBMs with log2 copy number <-1, indicating homozygous deletion of the 1p36 locus. **b**, DNA copy number correlates with messenger RNA expression; expression is highest in tumours with $n = 2$ copies (wild type) and lowest in tumours with $n = 0$ copies (null) of *ENO1*. **c**, The D423-MG cell line was identified as homozygously deleted by SNP arrays from the Wellcome Trust Sanger Institute data set. **d**, The complete absence of ENO1 protein in D423-MG and Gli56 cells was confirmed by western blotting. **e**, shRNA targeting *ENO2* (shENO2-3) but not scramble (shNT) in D423-MG *ENO1*-null cells ablated intracranial tumorigenesis *in vivo* ($n = 4$ mice per group).

observed marked toxicity in *ENO1*-null cells (Fig. 4a, c and Supplementary Fig. 7) and minimal impact on the *ENO1* wild-type controls, which show at least ten times greater enolase activity relative to the *ENO1*-null cells (because ENO1 accounts for 90% of the total cellular enolase activity[12]; Fig. 4b). Although the IC_{50} of PHAH is similar for ENO1 and ENO2 *in vitro* (data not shown) the greater toxicity of the inhibitor to *ENO1*-null cells (Gli56 and D423-MG) derives from the fact that in these cells enolase activity is already 90% lower than in wild-type ENO1 cell lines, and consequently, a much lower dose is required to decrease total enolase activity below the toxicity threshold. Further data indicate a direct relationship between the levels of enolase activity and the sensitivity to PHAH across different cell lines and in the same cell line with different levels of enforced enolase expression. First, U343 and D502-MG cells, which have intermediate levels of enolase activity (and ENO1 protein expression; Fig. 2d) compared with the other cell lines, have intermediate levels of sensitivity to PHAH (Fig. 4), which in the case of U343 can be rescued by ectopic overexpression of *ENO1* or *ENO2* (data not shown). A systematic titration of PHAH in D423-MG cell lines with varying levels of enforced ENO1 or ENO2 expression, shows a direct relationship between the level of enolase expression/activity and the ensuing resistance to PHAH (Supplementary Fig. 7). PHAH toxicity was also abrogated in Gli56 *ENO1*-null cells by ectopic expression of physiological levels of *ENO1* or overexpression of *ENO2* (Supplementary Fig. 7). Regarding the mechanism of toxicity, cell cycle and apoptosis analysis demonstrated that PHAH treatment for 48 h induced a marked decrease of S-phase cells followed by a marked increase of apoptosis in D423-MG but not in *ENO1* wild-type U373 cells (Supplementary Table 4). This effect was completely rescued by *ENO2* overexpression (data not shown). The fact that this growth inhibition and subsequent apoptosis is due to energy crisis is substantiated by a strong induction of phosphorylated 5′-AMP-activated protein kinase (AMPK) (at Thr 172)[29], which was observed in D423-MG but not in ENO1 wild-type cell lines (data not shown). It is tempting to speculate that this energy stress response exerts a protective effect, and thus the concomitant addition of an AMPK inhibitor together with PHAH could result in further toxicity. Finally, it is worth noting that *ENO1*-null cells do not show any greater sensitivity to other molecular-targeted therapies, such as a combination of receptor tyrosine kinase inhibitors[30] (lapatinib, sorafenib and PHA665752) (Supplementary Fig. 8) and rapamycin (data not shown) compared with wild-type *ENO1* cells. These data indicate that D423-MG cells are not broadly susceptible to other anticancer agents and that PHAH selectively targets *ENO1*-null GBM cells.

Discussion

In this study, we sought to determine the effect of collateral deletion of genes in tumour-suppressor loci that belong to redundant gene families playing cell-essential roles, and to assess whether extinction of remaining gene family members would create cancer-specific vulnerabilities. We provide genetic and pharmacological evidence that enolase 2 inhibition is lethal in cells with 1p36 homozygous deletion with collateral loss of *ENO1*, whereas *ENO1*-intact cells can rely on

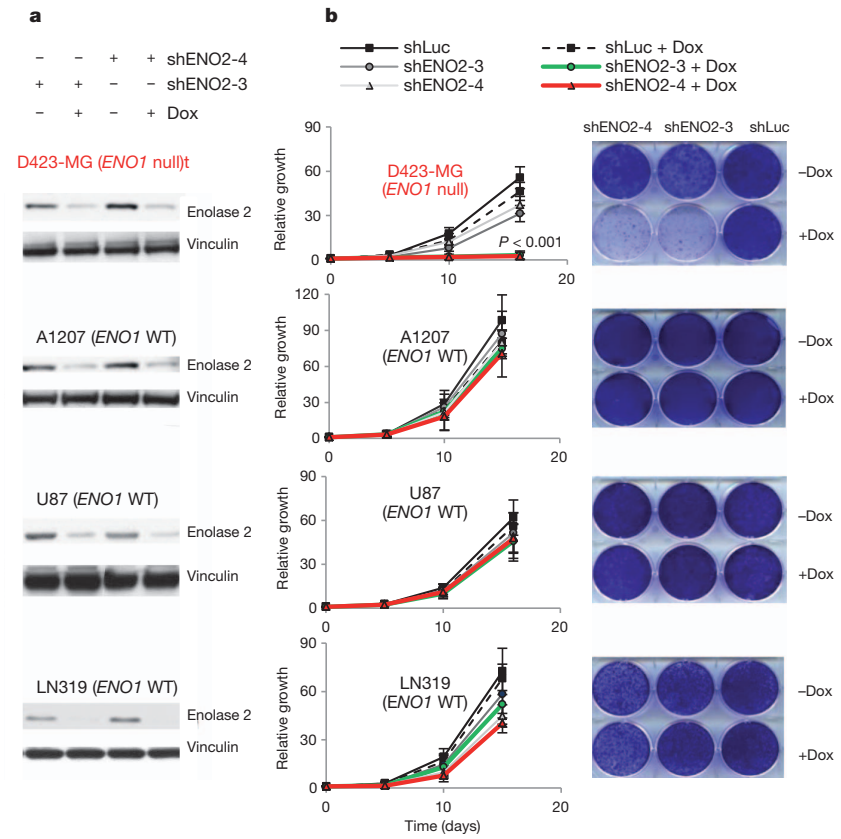

Figure 3 | shRNA ablation of *ENO2* affects *ENO1*-null but not *ENO1*-WT GBM cells. **a**, shRNA ablation by two independent doxycycline (Dox)-inducible TRIPZ hairpins against *ENO2* (shENO2-3, shENO2-4) resulted in >70% reduction in enolase 2 protein levels in both *ENO1* wild-type (WT) (A1207, U87 and LN319) and *ENO1*-null (D423-MG) cell lines. **b**, Ablation of *ENO2* markedly inhibited growth of *ENO1*-null but not wild-type *ENO1* cells, whereas non-targeting shRNA against luciferase (shLuc) had no effect in any cell line ($n = 3$ biological replicates, mean ± s.e.m., Student's *t*-test). Representative plates at the last time point of growth for cells infected with shLuc, shENO2-3 or shENO2-4, with or without Dox induction, are shown to the right of growth curves for each cell line.

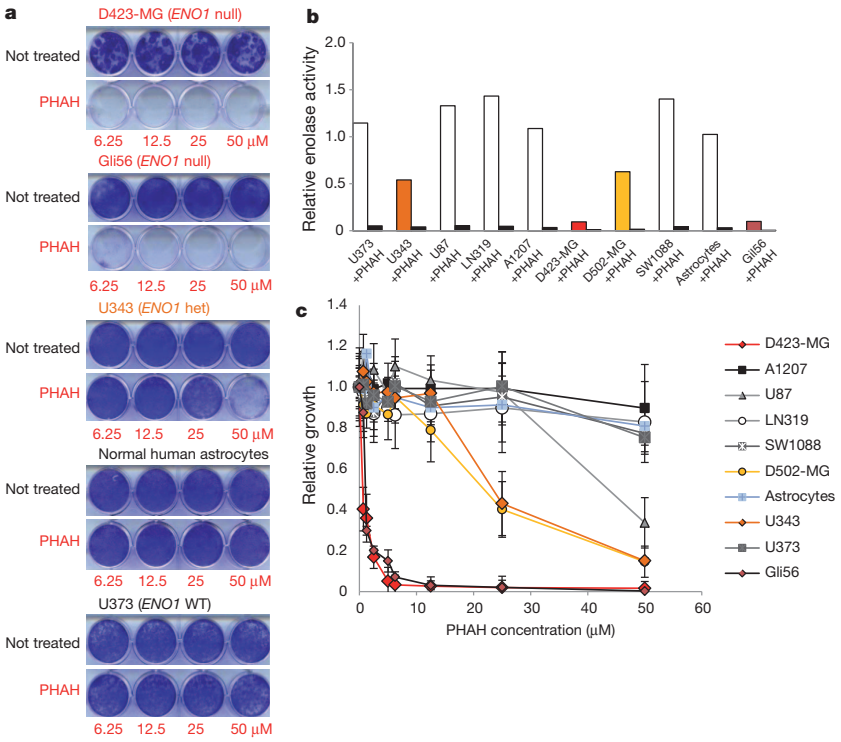

Figure 4 | Extreme sensitivity of *ENO1*-null cells to the pan-enolase inhibitor PHAH. **a**, D423-MG and Gli56 *ENO1*-null cell lines are highly sensitive to PHAH toxicity, whereas *ENO1* wild-type cell lines and normal astrocytes are not. Het, heterozygous deleted. **b**, The sensitivity of GBM lines to PHAH treatment correlated with their overall enolase activity. Pre-incubation of the lysates with 1 μM PHAH inhibited enolase enzymatic activity by >95% (average, $n = 2$ technical replicates). **c**, PHAH minimally affected the growth of *ENO1* wild-type GBM cells and normal astrocytes except at concentrations above 50 μM. Low PHAH concentrations stall the growth of *ENO1*-null cells, whereas cells with reduced *ENO1* expression (D502-MG and U343) showed intermediate sensitivity ($n = 4$ biological replicates, mean ± s.e.m.).

enolase 1 to undergo glycolysis and support survival. These findings are in agreement with genetic data from invertebrates[8–10]. Given that several homozygously deleted housekeeping genes can occur in the same deletion on 1p36 (for example, *H6PD*; Supplementary Table 1), it may be possible to increase the effectiveness and cancer cell-specific killing further by combining the inhibition of *ENO2* with that of another homologue of a simultaneously deleted housekeeping gene.

Attempts to therapeutically exploit general metabolic differences between normal and cancer cells, such as glucose addiction (the Warburg effect) and glutamine or serine addiction[16,31,32], remain areas of active preclinical investigation and clinical development. The approach described here is distinguished from these attempts in that it does not rely on any general aspect of cancer cell metabolism, but rather rests on genetically determined metabolic differences between normal and cancerous tissue to generate cancer cell-specific vulnerabilities. We propose that collateral vulnerability may be extended to other passenger homozygously deleted housekeeping genes in loci sustaining frequent deletion, such as 9p21 (*CDKN2A*) and 10q23 (*PTEN*), which contain members of functionally redundant housekeeping gene families (Table 1, Supplementary Table 1 and Supplementary Fig. 9). The strongest pharmacologically targetable candidates in this list are the homologues of the dual-function energy metabolism/iron regulator aconitase 1 (*ACO1*; 9p21) and the coenzyme A biosynthetic enzyme, pantothenate kinase 1 (*PANK1*; 10q23). Importantly, many of the compounds targeting the homologues of these passenger genes represent new molecular entities with respect to cancer treatment.

By one estimate, 11% of all protein-coding genes in the human genome are deleted in human cancers[33]. Thus, given the large number of homozygous deletions across many different cancer types spanning many hundreds of genes[33–36], the model described here for GBM should be applicable to the development of personalized treatments for many other cancer types.

METHODS SUMMARY

Cells were cultured using standard techniques in DMEM with 20% fetal bovine serum. shRNA experiments were conducted by lentiviral production through transient transfection of 293T cells followed by transduction in medium containing 4 $\mu g\,ml^{-1}$ polybrene and selection with 2 $\mu g\,ml^{-1}$ puromycin. shRNA expression was induced with 1 $\mu g\,ml^{-1}$ doxycycline and knockdown was tested by western blot. The shRNA-resistant ENO2 open reading frame was created by introducing silent mutations with the QuickChange site directed mutagenesis kit from Stratagene and then cloning into the pHAGE-CMV lentiviral vector. Cell proliferation experiments were performed using crystal violet staining, the CellTiter-Glo assay (Roche) and by measuring confluence using IncuCyte (Essen Bioscience). Orthotopic intracranial injections of D423-MG cells with and without ENO2 knockdown in severe combined immunodeficient (SCID) mice were performed as previously described[37]. Soft agar colony formation assay of these cells was performed using standard techniques by seeding 10^4 cells in 6-well plates. For the inhibitor studies, PHAH lithium salt was custom-synthesized by TCRS, following a previous protocol[28]. For the enolase activity assay, NADH oxidation was measured in a pyruvate kinase–lactate dehydrogenase coupled reaction as previously described[12]. For cell cycle studies, cells were incubated with or without PHAH for 48 h, stained with propidium iodide and sorted by flow cytometric analysis. For annexin V/7-AAD assays, cells were treated with or without PHAH for 96 h, stained with annexin V–phycoerythrin (PE) and 7-AAD, and evaluated for apoptosis by flow cytometry according to the manufacture's protocol (Biovision).

Full Methods and any associated references are available in the online version of the paper.

Received 16 January; accepted 15 June 2012.

1. The Cancer Genome Atlas Research Network. Comprehensive genomic characterization defines human glioblastoma genes and core pathways. *Nature* **455,** 1061–1068 (2008).
2. Druker, B. J. Translation of the Philadelphia chromosome into therapy for CML. *Blood* **112,** 4808–4817 (2008).
3. Guha, M. PARP inhibitors stumble in breast cancer. *Nature Biotechnol.* **29,** 373–374 (2011).
4. De Soto, J. A. & Deng, C. X. PARP-1 inhibitors: are they the long-sought genetically specific drugs for BRCA1/2-associated breast cancers? *Int. J. Med. Sci.* **3,** 117–123 (2006).
5. Weidle, U. H., Maisel, D. & Eick, D. Synthetic lethality-based targets for discovery of new cancer therapeutics. *Cancer Genomics Proteomics* **8,** 159–171 (2011).
6. Vavouri, T., Semple, J. I. & Lehner, B. Widespread conservation of genetic redundancy during a billion years of eukaryotic evolution. *Trends Genet.* **24,** 485–488 (2008).
7. Brookfield, J. F. Genetic redundancy. *Adv. Genet.* **36,** 137–155 (1997).
8. Costanzo, M. *et al.* The genetic landscape of a cell. *Science* **327,** 425–431 (2010).
9. DeLuna, A. *et al.* Exposing the fitness contribution of duplicated genes. *Nature Genet.* **40,** 676–681 (2008).
10. Deutscher, D., Meilijson, I., Kupiec, M. & Ruppin, E. Multiple knockout analysis of genetic robustness in the yeast metabolic network. *Nature Genet.* **38,** 993–998 (2006).
11. Poyner, R. R. & Reed, G. H. Structure of the bis divalent cation complex with phosphonoacetohydroxamate at the active site of enolase. *Biochemistry* **31,** 7166–7173 (1992).
12. Joseph, J., Cruz-Sanchez, F. F. & Carreras, J. Enolase activity and isoenzyme distribution in human brain regions and tumors. *J. Neurochem.* **66,** 2484–2490 (1996).
13. Stefanini, M. Chronic hemolytic anemia associated with erythrocyte enolase deficiency exacerbated by ingestion of nitrofurantoin. *Am. J. Clin. Pathol.* **58,** 408–414 (1972).
14. Kobayakawa, K. *et al.* Innate versus learned odour processing in the mouse olfactory bulb. *Nature* **450,** 503–508 (2007).
15. Comi, G. P. *et al.* β-enolase deficiency, a new metabolic myopathy of distal glycolysis. *Ann. Neurol.* **50,** 202–207 (2001).
16. Wise, D. R. & Thompson, C. B. Glutamine addiction: a new therapeutic target in cancer. *Trends Biochem. Sci.* **35,** 427–433 (2010).
17. Buszczak, M. *et al.* The carnegie protein trap library: a versatile tool for *Drosophila* developmental studies. *Genetics* **175,** 1505–1531 (2007).
18. Sonnichsen, B. *et al.* Full-genome RNAi profiling of early embryogenesis in *Caenorhabditis elegans*. *Nature* **434,** 462–469 (2005).
19. Henrich, K. O. *et al.* CAMTA1, a 1p36 tumor suppressor candidate, inhibits growth and activates differentiation programs in neuroblastoma cells. *Cancer Res.* **71,** 3142–3151 (2011).
20. Bagchi, A. & Mills, A. A. The quest for the 1p36 tumor suppressor. *Cancer Res.* **68,** 2551–2556 (2008).
21. Yin, D. *et al.* High-resolution genomic copy number profiling of glioblastoma multiforme by single nucleotide polymorphism DNA microarray. *Mol. Cancer Res.* **7,** 665–677 (2009).
22. Duncan, C. G. *et al.* Integrated genomic analyses identify ERRFI1 and TACC3 as glioblastoma-targeted genes. *Oncotarget* **1,** 265–277 (2010).
23. Kotliarov, Y. *et al.* High-resolution global genomic survey of 178 gliomas reveals novel regions of copy number alteration and allelic imbalances. *Cancer Res.* **66,** 9428–9436 (2006).
24. Peng, W. X. *et al.* Array-based comparative genomic hybridization analysis of high-grade neuroendocrine tumors of the lung. *Cancer Sci.* **96,** 661–667 (2007).
25. Mueller, W. *et al.* Downregulation of RUNX3 and TES by hypermethylation in glioblastoma. *Oncogene* **26,** 583–593 (2005).
26. Guha-Chowdhury, N., Clark, A. G. & Sissons, C. H. Inhibition of purified enolases from oral bacteria by fluoride. *Oral Microbiol. Immunol.* **12,** 91–97 (1997).
27. de A. S. & Navarro, M. V. *et al.* Structural flexibility in *Trypanosoma brucei* enolase revealed by X-ray crystallography and molecular dynamics. *FEBS J.* **274,** 5077–5089 (2007).
28. Anderson, V. E., Weiss, P. M. & Cleland, W. W. Reaction intermediate analogues for enolase. *Biochemistry* **23,** 2779–2786 (1984).
29. Jing, M. & Ismail-Beigi, F. Critical role of 5′-AMP-activated protein kinase in the stimulation of glucose transport in response to inhibition of oxidative phosphorylation. *Am. J. Physiol. Cell Physiol.* **292,** C477–C487 (2007).
30. Stommel, J. M. *et al.* Coactivation of receptor tyrosine kinases affects the response of tumor cells to targeted therapies. *Science* **318,** 287–290 (2007).
31. Possemato, R. *et al.* Functional genomics reveal that the serine synthesis pathway is essential in breast cancer. *Nature* **476,** 346–350 (2011).
32. Raj, L. *et al.* Selective killing of cancer cells by a small molecule targeting the stress response to ROS. *Nature* **475,** 231–234 (2011).
33. Bignell, G. R. *et al.* Signatures of mutation and selection in the cancer genome. *Nature* **463,** 893–898 (2010).
34. Taylor, B. S. *et al.* Integrative genomic profiling of human prostate cancer. *Cancer Cell* **18,** 11–22 (2010).
35. Cox, C. *et al.* A survey of homozygous deletions in human cancer genomes. *Proc. Natl Acad. Sci. USA* **102,** 4542–4547 (2005).
36. Tonon, G. *et al.* High-resolution genomic profiles of human lung cancer. *Proc. Natl Acad. Sci. USA* **102,** 9625–9630 (2005).
37. Zheng, H. *et al.* p53 and Pten control neural and glioma stem/progenitor cell renewal and differentiation. *Nature* **455,** 1129–1133 (2008).

Supplementary Information is linked to the online version of the paper at www.nature.com/nature.

Acknowledgements We thank K. Ligon, C. Maire, D. N. Louis, J. Kim and G. Mohapatra for sharing bioinformatics data from their tumour neurosphere banks. We also thank D. Bigner for sharing the D423-MG and D502-MG cell lines and D. N. Louis and J. Kim for sharing the Gli56 cell line. We thank G. Chu and D. Jakubosky for assistance with necropsy and histopathological analysis. F.L.M. was supported by a training grant from

the National Institutes of Health (NIH T32-CA009361) and a fellowship from the American Cancer Society (115992-PF-08-261-01-TBE). S.C. was supported by a Dana-Farber Cancer Institute/Harvard Cancer Center Myeloma SPORE career development grant. E.A. was supported by a Howard Hughes Medical Institute Medical Research Fellowship (57006984). V.M. was supported by a Harvard PRISE fellowship. M.A.L. was supported by a Diversity in Health-Related research award (3 P01 CA095616-08S1). F.L.M. thanks J. Mohr for assistance with figure preparations. We also thank K. Muller for assistance with manuscript editing. We thank all members of the DePinho and Chin laboratories for suggestions and discussions. This work is supported by the NIH (P01CA95616 to C.B., L.C. and R.A.D.) and by the Ben and Catherine Ivy Foundation (to R.A.D. and L.C.).

Author Contributions F.L.M. and R.A.D. generated the original hypothesis. F.L.M. performed all bioinformatics work, including scanning the TCGA data set (with initial assistance from J.H.) and identifying candidates for collateral lethality, with the exception of *KLHL9*, which was identified by E.F.-S. E.A. obtained the D423-MG cell line and designed and carried out the pLKO and pGIPZ shRNA experiments. S.C. designed and performed all shRNA experiments with the inducible vectors and rescue experiments. F.L.M. and E.A. identified PHAH, F.L.M. procured the compound, and F.L.M. and S.C. performed all inhibitor treatment experiments. L.N. generated shRNA-resistant constructs of *ENO2*. S.C., D.O. and E.F.-S. performed cell cycle and apoptosis assays. R.N., V.M., D.E., P.D. and J.L. performed cell culture, crystal violet staining, western blotting and associated experiments and assisted in the preparation of figures. C.B. provided extensive unpublished genomic data and reagents from his primary brain tumour and neurosphere bank for Supplementary Table 1. E.A., M.A.L., B.H. and G.G. performed tumour cell injections. D.H., E.S., L.K., Y.A.W. and L.C. provided intellectual contributions throughout the project. F.L.M., E.A., S.C., Y.A.W., L.C. and R.A.D. wrote the paper.

Author Information Reprints and permissions information is available at www.nature.com/reprints. The authors declare no competing financial interests. Readers are welcome to comment on the online version of this article at www.nature.com/nature. Correspondence and requests for materials should be addressed to R.D. (rdepinho@mdanderson.org).

METHODS

Cell culture. The cell lines D423-MG (1p36 homozygously deleted, including *ENO1*) and D502-MG (1p36 homozygously deleted, excluding *ENO1*) were provided by D. Bigner[22]. (D423 and D502 are referred to as H423 and H502, respectively, in ref. 22, but as D423-MG and D502-MG in the Wellcome Trust Sanger Institute database (http://www.sanger.ac.uk), the nomenclature we adopt here). Gli56 was obtained from D. N. Louis as described in ref. 25. The deletion in D423-MG spans the *CAMTA1*, *VAMP3*, *PER3*, *UTS2*, *TNFRSF9*, *PARK7*, *ERRFI1*, *SLC45A1*, *RERE*, *ENO1*, *CA6*, *SLC2A5*, *GPR157*, *MIR34A*, *H6PD*, *SPSB1* and *SLC25A33* genes, whereas the deletion in Gli56 spans the *UTS2*, *TNFRSF9*, *PARK7*, *ERRFI1*, *SLC45A1*, *RERE*, *ENO1*, *CA6*, *SLC2A5*, *GPR157*, *MIR34A*, *H6PD*, *SPSB1*, *SLC25A33*, *TMEM201*, *C1orf200*, *PIK3CD*, *CLSTN1*, *CTNNBIP1*, *LZIC*, *NMNAT1*, *RBP7* and *UBE4B* loci. Cells were cultured in DMEM with 20% fetal bovine serum (FBS). For comparison, the cell lines U87, LN319, SW1088, U343, U373 and A1207 were grown under the same conditions. Normal human astrocytes were obtained from ScienCell.

shRNA knockdown of *ENO2* expression. We screened 22 hairpins targeting *ENO2* and found four independent ones that reduced protein levels by $<50\%$. Two of these hairpins were in the pLKO.1 vector (shENO2-1 and shENO2-2), and the remaining two were in the Expression Arrest GIPZ (shENO2-3) and TRIPZ (shENO2-4) shRNAmir vectors (Open Biosystems). The *ENO2* shRNA sequences are as follows: shENO2-1: 5′-CAAGGGAGTCATCAAGGACAA-3′; NCBI accession NM_001975. shENO2-2: 5′-CGCCTGGCTAATAAGGC TTTA-3′; NM_001975. shENO2-3: 5′-CGGCCTTCAACGTGATCAA-3′; NM_001975. shENO2-4: 5′-GGGACTGAGAACAAATCCA-3′; NM_001975.

The hairpin in the GIPZ vector was cloned into the TRIPZ vector using a protocol provided by the manufacturer. The TRIPZ vector is a doxycycline-inducible system with a red fluorescent protein reporter that is expressed only after doxycycline induction. Recombinant lentiviral particles were produced by transient transfection of 293T cells following a standard protocol. In brief, 72 μg of the shRNA plasmid, 54 μg of delta 8.9 plasmid and 18 μg of the VSVG plasmid were transfected using FuGene (Roche) into 293T cells plated in 245-mm^2 dishes. Viral supernatant was collected 72 h after transfection, concentrated by ultracentrifugation at 90,000*g*, and resuspended in cell growth medium. For transduction, viral solutions were added to cell culture medium containing 4 μg ml^{-1} polybrene; 48 h after infection, cells were selected using 2 μg ml^{-1} puromycin and tested for *ENO2* knockdown by western blotting.

Proliferation assays and anchorage-independent growth. Cell growth of shRNA- or PHAH-treated cell lines was assayed either through crystal violet staining or using the Promega CellTiter-Glo proliferation kit (Roche) or alternatively, *in vivo*, by measuring confluence with the IncuCyte (Essen BioScience). Growth curves using the IncuCyte were generated by imaging every 2 h with quadruplicate replicates. For crystal violet assays, 10^4 cells were seeded in a 6-well plate for each time point. At the indicated time point, cells were fixed with 10% formalin and stained with crystal violet solution for 1 h. Dye extraction was performed using 10% acetic acid solution, and absorbance was read at 590 nm. CellTiter-Glo experiments were performed according to the manufacturer's instructions; 10^3 cells per well were plated in a 96-well plate for each time point, and luminescence readings were taken every 24 h. All experiments were performed in triplicate. Soft agar (anchorage-independent) growth was monitored in 6-well plates seeded with 10^4 cells of the indicated genotype. The medium contained DMEM with 10% FBS; the top agar contained 0.4% low melting agarose, whereas the bottom agar contained 1% low melting agarose. Growth was monitored by fluorescence (green fluorescent protein, GFP) and after 28 days colonies were stained with iodonitrotetrazolium chloride (Sigma-Aldrich) and counted.

Orthotopic brain tumour formation. The *in vivo* tumorigenic potential of D423-MG cells transduced with non-targeting hairpin or shENO2-3 delivered through pGIPZ was determined as previously described[37]. SCID mice (Charles River) under deep anaesthesia were placed into a stereotactic apparatus equipped with a *z*-axis (Stoelting). Then, 3×10^5 cells were injected intracranially into the right caudate nucleus, 3 mm below the surface of the brain, using a 10-μl Hamilton syringe. The animals were followed daily for the development of neurological deficits. All mice experiments were performed with the approval of the Harvard Cancer Center and Dana-Farber Cancer Institute Institutional Animal Care and Use Committee.

Enolase activity assay. Enolase activity was measured by NADH oxidation in a pyruvate kinase–lactate dehydrogenase coupled assay as previously described[12]. In brief, cells were lysed in 20 mM Tris-HCl, 1 mM EDTA and 1 mM β-mercaptoethanol (pH 7.4), and homogenized using a Polytron homogenizer three times for a period of 10 s followed by sonication. Enolase activity was recorded by measuring oxidation of NADH either spectrophotometrically by absorbance at 340 nm or fluorescently by excitation at 340 nm and emission at 460 nm.

Western blotting. After two washes with PBS, cells were incubated in RIPA buffer for 15 min with gentle shaking. Lysates were then collected, sonicated and centrifuged at 20,000*g* for 10 min at 4 °C. SDS–PAGE and western blotting were performed as described previously[37]. The following antibodies were used: enolase 1 (3810), enolase 2 (9536), GAPDH (3683) and phosphor-AMPK Thr 172 (2535) from Cell Signaling Technologies, and vinculin from Sigma-Aldrich.

Inhibitor studies. PHAH lithium salt was custom-synthesized by TCRS, following the protocol described previously[28]. Structure and purity were verified by NMR. PHAH was dissolved in PBS at 50 mM stock and stored frozen at −80 °C until use. Given the instability of the compound, the medium was replaced every 5 days and fresh inhibitor added with fresh medium. Rapamycin, sorafenib, lapatinib were obtained from LC Laboratories and PHA665752 from Tocris Bioscience, respectively.

Ectopic expression of *ENO1*, *ENO2* and shRNA-resistant *ENO2*. Rescue of the phenotypic effects of knocking down *ENO2* in the cell line D423-MG was performed by overexpressing an shRNA-resistant form of *ENO2*. In brief, six silent mutations were introduced into the *ENO2* coding region targeted by shENO2-4, using the QuikChange site-directed mutagenesis kit (Stratagene). The shRNA-resistant *ENO2* coding region was cloned into the pHAGE-CMV lentiviral vector (a gift from D. N. Kotton) and overexpressed in the D423-MG cell line carrying shENO2-4, in the presence or absence of doxycycline. As a control, the same cell line was infected with a lentiviral vector carrying the GFP gene. For the ectopic re-expression of *ENO1* or *ENO2*, sequenced verified cDNA clones were gateway cloned into the pHAGE-CMV lentiviral vector and lentivirally transduced into glioma cell lines as described earlier.

Cell cycle analysis. The D423-MG and U373 cell lines were treated for 48 h in the presence or absence of PHAH (25 μM) and fixed in 75% ethanol at −20 °C overnight. The next day, the cells were washed with cold PBS, treated with 100 μg of RNase A (Qiagen), and stained with 50 μg of propidium iodide (Roche). Flow cytometric acquisition was performed using a three-colour FACScan flow cytometer and CellQuest software (Becton Dickinson). For each sample, 10^4 events were gated. Data analysis was performed using ModFit LT (Verity Software House).

Annexin V/7-AAD assay for apoptosis. The D423-MG and U373 cell lines were treated for 96 h in the presence or absence of PHAH (25 μM). For Annexin V/7-AAD assay cells were stained with annexin V–PE and 7-AAD, and evaluated for apoptosis by flow cytometry according to the manufacturer's protocol (Biovision). The apoptotic cells were determined using a Becton Dickinson FACScan cytometer. Both early apoptotic (annexin V-positive and 7-AAD-negative) and late apoptotic (annexin V-positive and 7-AAD-positive) cells were included in cell death determinations.

CORRIGENDUM

doi:10.1038/nature14609

Corrigendum: Passenger deletions generate therapeutic vulnerabilities in cancer

Florian Muller, Simona Colla, Elisa Aquilanti, Veronica E. Manzo, Giannicola Genovese, Jaclyn Lee, Daniel Eisenson, Rujuta Narurkar, Pingna Deng, Luigi Nezi, Michelle Lee, Baoli Hu, Jian Hu, Ergun Sahin, Derrick Ong, Eliot Fletcher-Sananikone, Dennis Ho, Lawrence Kwong, Cameron Brennan, Y. Alan Wang, Lynda Chin & Ronald A. DePinho

Nature **488,** 337–342 (2012); doi:10.1038/nature11331

In this Article, during the preparation of Figures 2d and 3a, we processed digital western blot scans to remove duplicate or otherwise irrelevant lanes from single-blot images. Although all excisions/mergers originated from the same gel, these figure constructions should have been explicitly pointed out. Here we present the unprocessed scans (Supplementary Information) and amended figures (Figs 1 and 2). Figure 1 of this Corrigendum shows the corrected Fig. 2d, in which a duplicate run of cell line D423-MG (lane 2 in the original) was excised between cell lines D502-MG and U343 (lanes 1 and 3 in the original) and the ensuing halves of the blot were spliced together (lanes 1 and 3 in the original blot). This is now indicated by a dashed line. Similarly, Fig. 2 of this Corrigendum shows the corrected Fig. 3a, in which for the cell line U87, an additional non-targeting short hairpin RNA control (original lanes 7 and 8) was excised with the remaining halves of the blot and merged, which is now indicated by a dashed line. We also note that in the published Fig. 3a, lanes 1 and 2 of the original U87 vinculin blot were accidentally used as the loading control for shENO2-4 (lanes 9 and 10 of the original unprocessed ENO2 blot in the Supplementary Information), and lanes 9 and 10 of the vinculin blot should have been used as the correct loading control lanes. The correct loading control lanes are now shown (Supplementary Information). None of these corrections alter the original meaning of the experiments, their results, their interpretation, nor the conclusions of the paper. We apologize for any confusion this may have caused to the readers of *Nature*.

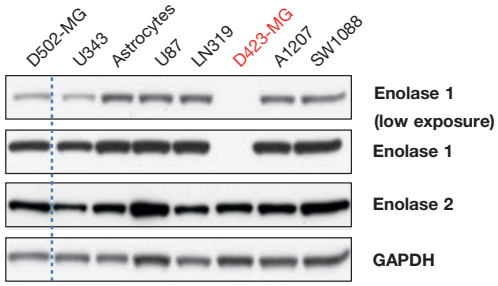

Figure 1 | This is the corrected Fig. 2d of the original Article, with excision indicated.

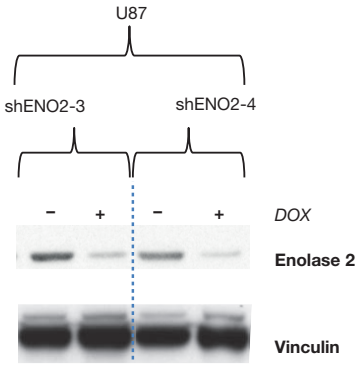

Figure 2 | This is the corrected Fig. 3a of the original Article, with excision indicated.

Supplementary Information is available in the online version of this corrigendum.